



**Omnidirectional Printing of Flexible, Stretchable,  
and Spanning Silver Microelectrodes**

Bok Y. Ahn, *et al.*  
*Science* **323**, 1590 (2009);  
DOI: 10.1126/science.1168375

**The following resources related to this article are available online at  
[www.sciencemag.org](http://www.sciencemag.org) (this information is current as of March 20, 2009 ):**

**Updated information and services**, including high-resolution figures, can be found in the online version of this article at:

<http://www.sciencemag.org/cgi/content/full/323/5921/1590>

**Supporting Online Material** can be found at:

<http://www.sciencemag.org/cgi/content/full/1168375/DC1>

This article **cites 25 articles**, 7 of which can be accessed for free:

<http://www.sciencemag.org/cgi/content/full/323/5921/1590#otherarticles>

This article appears in the following **subject collections**:

Materials Science

[http://www.sciencemag.org/cgi/collection/mat\\_sci](http://www.sciencemag.org/cgi/collection/mat_sci)

Information about obtaining **reprints** of this article or about obtaining **permission to reproduce this article** in whole or in part can be found at:

<http://www.sciencemag.org/about/permissions.dtl>

## References and Notes

- N. W. Ashcroft, N. D. Mermin, *Solid State Physics* (Brooks Cole, New York, 1976).
- A. Y. Ganin *et al.*, *Nat. Mater.* **7**, 367 (2008).
- M. S. Nam, A. Ardavan, S. J. Blundell, J. A. Schlueter, *Nature* **449**, 584 (2007).
- A. Comanac, L. De'Medici, M. Capone, A. J. Millis, *Nat. Phys.* **4**, 287 (2008).
- M. Capone, M. Fabrizio, C. Castellani, E. Tosatti, *Rev. Mod. Phys.*, in press; <http://arxiv.org/abs/0809.0910> (2008).
- M. Capone, M. Fabrizio, C. Castellani, E. Tosatti, *Science* **296**, 2364 (2002).
- O. Gunnarsson, E. Koch, R. M. Martin, *Phys. Rev. B* **54**, R11026 (1996).
- O. Gunnarsson, *Rev. Mod. Phys.* **69**, 575 (1997).
- K. Tanigaki *et al.*, *Nature* **352**, 222 (1991).
- P. Dahlke, M. S. Denning, P. F. Henry, M. J. Rosseinsky, *J. Am. Chem. Soc.* **122**, 12352 (2000).
- T. T. M. Palstra *et al.*, *Solid State Commun.* **93**, 323 (1995).
- S. Saito, K. Umemoto, S. G. Louie, M. L. Cohen, *Solid State Commun.* **130**, 335 (2004).
- See supporting material on Science Online.
- C. P. Schlichter, *Principles of Magnetic Resonance* (Springer, Heidelberg, 1990).
- C. H. Pennington, V. A. Stenger, *Rev. Mod. Phys.* **68**, 855 (1996).
- N. Sato *et al.*, *Phys. Rev. B* **58**, 12433 (1998).
- K. Prassides *et al.*, *J. Am. Chem. Soc.* **121**, 11227 (1999).
- G. R. Darling, A. Y. Ganin, M. J. Rosseinsky, Y. Takabayashi, K. Prassides, *Phys. Rev. Lett.* **101**, 136404 (2008).
- O. Gunnarsson, J. E. Han, E. Koch, V. H. Crespi, *Struct. Bonding* **114**, 71 (2005).
- T. Kambe, K. Kajiyoshi, M. Fujiwara, K. Oshima, *Phys. Rev. Lett.* **99**, 177205 (2007).
- L. F. Chibotaru, *J. Mol. Struct.* **838**, 53 (2007).
- T. Kawamoto, *Solid State Commun.* **101**, 231 (1997).
- J. Curely, *Monatsh. Chem.* **136**, 987 (2005).
- S. Margadonna, K. Prassides, H. Shimoda, T. Takenobu, Y. Iwasa, *Phys. Rev. B* **64**, 132414 (2001).
- A. Y. Ganin *et al.*, *J. Am. Chem. Soc.* **128**, 14784 (2006).
- Y. Takabayashi, A. Y. Ganin, M. J. Rosseinsky, K. Prassides, *Chem. Commun.* **2007**, 870 (2007).
- Y. Iwasa, T. Takenobu, *J. Phys. Condens. Matter* **15**, R495 (2003).
- Y. Iwasa, T. Kaneyasu, *Phys. Rev. B* **51**, 3678 (1995).
- We thank the UK Engineering and Physical Sciences Research Council for funding under EP/C511794 and GR/S77820 and for access to the synchrotron x-ray facilities at the European Synchrotron Radiation Facility (where we thank A. N. Fitch for assistance on beamline ID31) and to the muon facilities at ISIS (where we thank S. R. Giblin for assistance on the MuSR instrument). We also thank Spring-8 for access to the synchrotron x-ray facilities.

## Supporting Online Material

[www.sciencemag.org/cgi/content/full/323/5921/1585/DC1](http://www.sciencemag.org/cgi/content/full/323/5921/1585/DC1)

Materials and Methods

Figs. S1 to S4

References

1 December 2008; accepted 2 February 2009

10.1126/science.1169163

# Omnidirectional Printing of Flexible, Stretchable, and Spanning Silver Microelectrodes

Bok Y. Ahn,<sup>1,2</sup> Eric B. Duoss,<sup>1,2</sup> Michael J. Motala,<sup>1,3</sup> Xiaoying Guo,<sup>1,2</sup> Sang-Il Park,<sup>1,2</sup> Yujie Xiong,<sup>1,2</sup> Jongseung Yoon,<sup>1,2</sup> Ralph G. Nuzzo,<sup>1,3</sup> John A. Rogers,<sup>1,2,3</sup> Jennifer A. Lewis<sup>1,2\*</sup>

Flexible, stretchable, and spanning microelectrodes that carry signals from one circuit element to another are needed for many emerging forms of electronic and optoelectronic devices. We have patterned silver microelectrodes by omnidirectional printing of concentrated nanoparticle inks in both uniform and high-aspect ratio motifs with minimum widths of approximately 2 micrometers onto semiconductor, plastic, and glass substrates. The patterned microelectrodes can withstand repeated bending and stretching to large levels of strain with minimal degradation of their electrical properties. With this approach, wire bonding to fragile three-dimensional devices and spanning interconnects for solar cell and light-emitting diode arrays are demonstrated.

Printed electronics offer an attractive alternative to conventional technologies by enabling the creation of large-area, flexible devices at low cost (1). Although there are options available for electronic materials—including conducting polymers (2, 3), inorganic semiconductors (4, 5) and carbon nanotubes (6, 7)—the ability to print low-resistance electrodes with fine resolution in high-aspect ratio layouts, and possibly spanning three dimensions, is a technologically important goal. Many applications, including solar cell metallization (8), flexible displays (9), radio frequency identification tags (10), and antennas (11), would benefit from this capability. Conventional approaches, such as screen-printing (12) and inkjet printing (13),

produce low-aspect ratio features that must be supported by the underlying substrate or device, making it impossible to pattern spanning elements in- or out-of-plane.

Direct ink writing offers an attractive alternative for meeting the demanding design rules and form factors required for metallic electrodes in printed electronic and optoelectronic devices.

In this filamentary printing approach, a concentrated ink is extruded through a tapered cylindrical nozzle that is translated using a three-axis, motion-controlled stage with nanoscale precision (Fig. 1A) (14). Yet, several limitations remain to be overcome. To date, the minimum feature size obtained with the use of nanoparticle inks is 100  $\mu\text{m}$  (15). In addition, the inks had to be deposited in a non-wetting oil reservoir to avoid nozzle clogging. Finally, ink deposition has been confined solely to the  $xy$  plane, such that three-dimensional (3D) structures are assembled in a layerwise sequence. We report the omnidirectional printing of flexible, stretchable, and spanning microelectrodes using concentrated silver nanoparticle inks that readily flow through micro-nozzles in air.

Metallic nanoparticles are typically synthesized in solution by the reduction of metal precursors in the presence of surface capping agents (16–19). Through a multistep approach (fig. S1), we prepared highly concentrated silver nanoparticle inks using an aqueous system that contains silver nitrate as the silver precursor, poly(acrylic acid) (PAA) as the capping agent, and diethanolamine as the reducing agent (20, 21). The components are first mixed under ambient conditions to create a population of very fine (~5-nm) silver nanoparticles. This particle

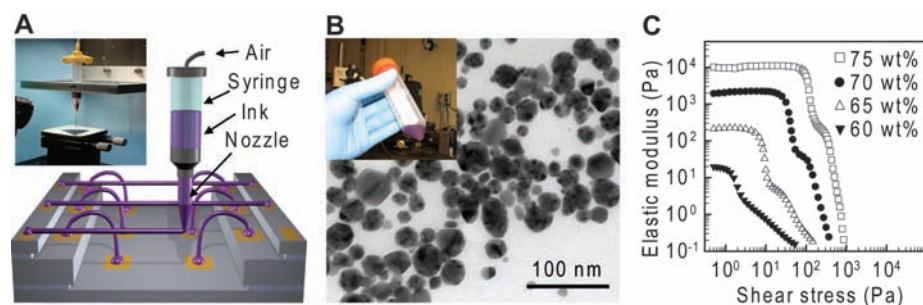


**Fig. 1.** (A) Schematic diagram illustrating omnidirectional printing and optical image of apparatus used (inset). (B) Transmission electron microscopy image of the synthesized silver nanoparticles and optical image of the concentrated ink (inset). (C) Shear elastic modulus as a function of shear stress for silver nanoparticle inks of varying solids loading.

<sup>1</sup>Frederick Seitz Materials Research Laboratory, University of Illinois at Urbana-Champaign, Urbana, IL 61801, USA.

<sup>2</sup>Department of Materials Science and Engineering, University of Illinois at Urbana-Champaign, Urbana, IL 61801, USA. <sup>3</sup>Department of Chemistry, University of Illinois at Urbana-Champaign, Urbana, IL 61801, USA.

\*To whom correspondence should be addressed. E-mail: [jalewis@illinois.edu](mailto:jalewis@illinois.edu)

population is ripened by heating the solution to 60°C (Fig. 1B). Ethanol, a poor solvent for the PAA-coated nanoparticles, is added to induce rapid particle coagulation. Next, the ink is centrifuged to achieve the desired solids loading [ $\geq 70$  weight percent (wt %) silver nanoparticles], as shown in the inset of Fig. 1B. Finally, ethylene glycol is added as a humectant, which allows the ink to be patterned in air without clogging.

We have synthesized a broad range of silver nanoparticle inks and found that those with a solids loading between 70 and 85 wt %, a mean particle size of  $20 \pm 5$  nm, and a particle size distribution between 5 and 50 nm exhibited both optimal flow behavior through fine deposition nozzles (1 to 30  $\mu\text{m}$ ) and low resistivity at modest annealing temperatures ( $\geq 200^\circ\text{C}$ ). Figure 1C shows the elastic modulus ( $G'$ ) as a function of shear stress for silver nanoparticle inks of varying solids loading. In the linear viscoelastic region,  $G'$  rises nearly three orders of magnitude as the nanoparticle content increases from 60 to 75 wt %. A minimum  $G'$  of 2000 Pa is required to produce spanning features, which occurs at a silver nanoparticle concentration of  $\sim 70$  wt %. These highly concentrated inks can

be stored under ambient conditions for weeks without any noticeable change in printing behavior (fig. S2).

To demonstrate the printing technique, we have patterned planar microelectrode arrays onto a silicon wafer by depositing silver nanoparticle ink (71-wt % solids) through 1-, 5-, and 10- $\mu\text{m}$  cylindrical nozzles (Fig. 2A). Printed features with aspect ratios ( $h/w$ , where  $h$  is height and  $w$  is width) of  $\sim 0.7$  are obtained in a single-pass, and a minimum width of  $\sim 2$   $\mu\text{m}$  is achieved with the use of a 1- $\mu\text{m}$  nozzle. In addition, high-aspect ratio features are patterned in a layerwise manner, and their width and height are defined solely by the nozzle diameter and number of printed layers, respectively (Fig. 2, B and C).

The microstructural evolution of the printed silver microelectrodes as a function of annealing temperature is shown in Fig. 2D. As the temperature increases from 150° to 550°C, the microelectrodes undergo simultaneous loss of organics, grain growth, and densification. Thermogravimetric analysis reveals that the organic species are removed by  $\sim 400^\circ\text{C}$  (fig. S1), whereas scanning electron microscopy (SEM) shows that their average grain size increases from  $\sim 180$  nm at 150°C to 3  $\mu\text{m}$  at 550°C, as a total volumetric shrinkage of

$\sim 30\%$  occurs. Concomitantly, their electrical resistivity,  $\rho$ , decreases sharply over this temperature range (Fig. 2E). Upon annealing at 250°C for short times ( $\leq 30$  min), the patterned microelectrodes exhibit an electrical resistivity of  $5.2 \times 10^{-5}$  ohm-cm, approaching the value of bulk silver ( $10^{-6}$  ohm-cm). In contrast, microelectrodes annealed at 150°C require several hours ( $\geq 25$  hours) to reach  $\rho \sim 10^{-3}$  ohm-cm, a value comparable to that observed for doped poly(3,4-ethylenedioxythiophene)/poly(styrenesulfonate), a widely used organic conductor (22, 23).

To demonstrate the flexibility of the printed features, we patterned a series of interdigitated microelectrode arrays on a polyimide substrate. Figure 3A shows optical and SEM images of the printed silver microelectrodes after annealing at 200°C for 3 hours, followed by wrapping the patterned substrate around a scintillation vial with a bending radius of 14 mm. Solid contact pads (1 by 1 mm) connected to linear electrode features are formed with a 30- $\mu\text{m}$  nozzle, to which interdigitated features are patterned with a 5- $\mu\text{m}$  nozzle (Fig. 3A, top right). These elaborate structures require the initiation and cessation of ink flow multiple times during the printing process (Fig. 3A, bottom right).

To investigate the effects of mechanical bending on electrical performance, we used a custom-built mechanical stage coupled to a micropositioner to carry out bend tests (fig. S3A). For this experiment, a linear array of 10 silver microelectrodes ( $w = 23$   $\mu\text{m}$ ,  $h = 12$   $\mu\text{m}$ , and length  $l = 1$  cm) spaced 0.5 mm apart are printed on a 25- $\mu\text{m}$ -thick polyimide sheet and annealed at 200°C for 3 hours in air before mechanical testing. Their electrical resistivity is measured as a function of bending radius from  $\pm 11$  mm to  $\pm 5$  mm, and the reported  $\rho$  values are averaged from 10 electrodes. In the first bend cycle,  $\rho$  is found to be  $6.23 \pm 4.40 \times 10^{-4}$ ,  $2.11 \pm 0.91 \times 10^{-4}$ , and  $2.00 \pm 1.11 \times 10^{-4}$  ohm-cm in tension (convex), unstrained (flat), and compression (concave), respectively (Fig. 3B). An approximately twofold change in electrical resistivity is observed after 1000 bend cycles at the smallest radius of  $\pm 5$  mm (Fig. 3C), where  $(\rho_{1000} - \rho_0)/\rho_0$  is 2.17, 1.66, and 1.67 for the tensile, unstrained, and compressive states, respectively.

Ultrathin ( $\sim 20$  nm) metal films deposited onto prestrained, stretchable substrates can form wavy buckles and arches upon relaxation of the substrate (24). These configurations are even observed in brittle semiconductor materials, such as silicon, because of the differences in mechanical behavior between ultrathin and bulk materials (25). The built-in slack enables mechanical stretching while preserving the desired electronic properties. Stretchable, wavy, and arched architectures can also be created out of nonbrittle materials that are not ultrathin, particularly for ductile metals. Figure 3D shows stretchable silver arches formed by printing a spanning silver microelec-

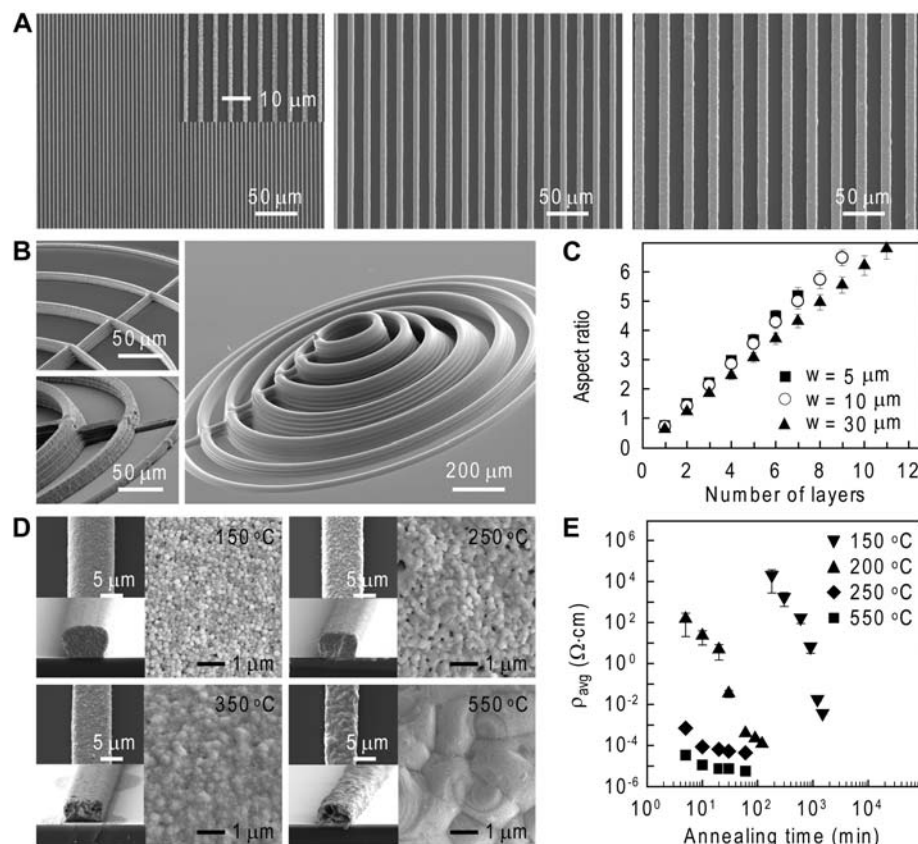


**Fig. 2.** (A) SEM images of planar arrays of silver microelectrodes patterned with 1- (left), 5- (center), and 10- $\mu\text{m}$  (right) nozzles. (B) SEM images of multilayer silver microelectrodes patterned with 5- (top left), 10- (bottom left), and 30- $\mu\text{m}$  (right) nozzles. (C) Aspect ratio as a function of number of printed layers for the silver microelectrodes shown in Fig. 2B. (D) SEM images of silver microelectrodes patterned with a 15- $\mu\text{m}$  nozzle as a function of annealing temperature. (E) Electrical resistivity of silver microelectrodes as a function of annealing temperature and time. Error bars indicate the SD measured from three electrodes.

trode onto a prestrained spring (inset) that is then released to form the desired arches. The specimens are annealed at varying temperatures, and a silicone adhesive is subsequently printed onto the spring at the microelectrode contact points to ensure good adhesion and accurate resistivity measurements. The electrical resistivity of the

silver microelectrode arches annealed at different temperatures is plotted as a function of strain  $[(L - L_0)/L_0 \times 100\%]$  in Fig. 3E. The maximum strain increases with increasing annealing temperature from 8% at 200°C to 25% at 550°C, as the microelectrodes transform to a bulklike ductility. Straining these microelectrodes up to 200

cycles does not result in fatigue-induced failure at the contact points (Fig. 3F).

We have provided a few examples of conductive features that can be patterned across unsupported regions in three dimensions. It is possible to vertically print microelectrodes with arbitrary height and angle (fig. S4). Figure 4A shows wire bonding of silver microelectrodes onto the surface of a thin silicon spherical shell assembled by lithographically patterning, releasing, and folding a 2- $\mu\text{m}$  silicon layer in the desired 3D form (fig. S5). Unlike conventional techniques (26), our approach allows fine silver microwires ( $\sim 10\ \mu\text{m}$ ) to be bonded with minimal contact pressure on both flat and curved surfaces, which is highly advantageous for delicate devices.

When combined with other processes (for instance, photolithography and transfer printing), our ink writing technique enables the heterogeneous integration of dissimilar materials (8, 27). To further highlight this capability, we have patterned interconnects for both solar microcell and light-emitting diode (LED) arrays. As a first example, we patterned silver microelectrodes ( $w = 15\ \mu\text{m}$ ,  $h = 13\ \mu\text{m}$ ) onto a silicon solar microcell ( $w = 45\ \mu\text{m}$ ,  $h = 26\ \mu\text{m}$ , and  $l = 2\ \text{mm}$ ) array, in which each photovoltaic element is separated by a 33- $\mu\text{m}$  gap (fig S6). Figure 4B shows that the silver microelectrodes span the unsupported regions between each solar microcell without deformation. We also find that these inks can span unsupported gaps that are extraordinarily wide, up to 1.0 cm across (fig. S7). The current ( $I$ )–voltage ( $V$ ) response from an individual silicon solar microcell and 14 interconnected microcells under a simulated air mass 1.5 illumination condition of  $1000\ \text{W}\cdot\text{m}^{-2}$  is shown in Fig. 4C. Because of their fine lateral dimensions, these conductive tracks can be spaced closely together, thereby blocking less incoming light and allowing more current to be drawn from each solar cell (28).

As a final demonstration, we exploited omnidirectional printing to create interconnects for the gallium arsenide–based LED array (4-by-4 pixels, where each pixel is 500 by 500 by 2.5  $\mu\text{m}$  and spaced 200  $\mu\text{m}$  apart) shown in Fig. 4D. The ability to print out-of-plane enables the microelectrodes to directly cross pre-existing patterned features through the formation of spanning arches (Fig. 4E, top left). Typically, insulating layers or bypass electrode arrays are required in conventional layouts. Figure 4E (top right) shows silver micro-arches printed on a gold pad (80 by 80  $\mu\text{m}$ ) on a LED pixel. Figure 4E (bottom) displays the LED array, emitting uniform red light under an applied bias of 6 V from a single pixel, after annealing at 200°C for 3 hours. The utility of this approach is further established by printing spanning arches onto commercially available gallium nitride LED chips (fig. S8).

In summary, we have demonstrated the omnidirectional printing of flexible, stretchable, and spanning microelectrodes with the use of tailored silver nanoparticle inks. By carefully controlling

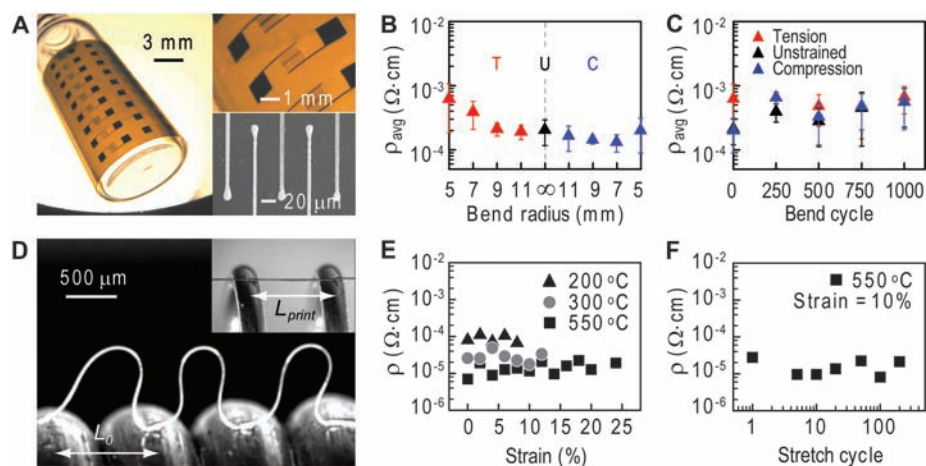


**Fig. 3.** (A) Optical and SEM images of silver microelectrodes patterned on a polyimide substrate with a bend radius of 14 mm. (B) Electrical resistivity of the silver microelectrodes as a function of bend radius under tension (T), unstrained (U), and compression (C). (C) Electrical resistivity of the silver microelectrodes as a function of bend cycle at a bend radius of  $\pm 5$  mm. (D) Optical image of stretchable silver arches printed onto a spring. (E) Electrical resistivity of the stretchable silver microelectrode arches as a function of strain and annealing temperature. (F) Electrical resistivity of the stretchable silver microelectrode arches as a function of strain cycle. Error bars indicate the SD measured from 10 electrodes.

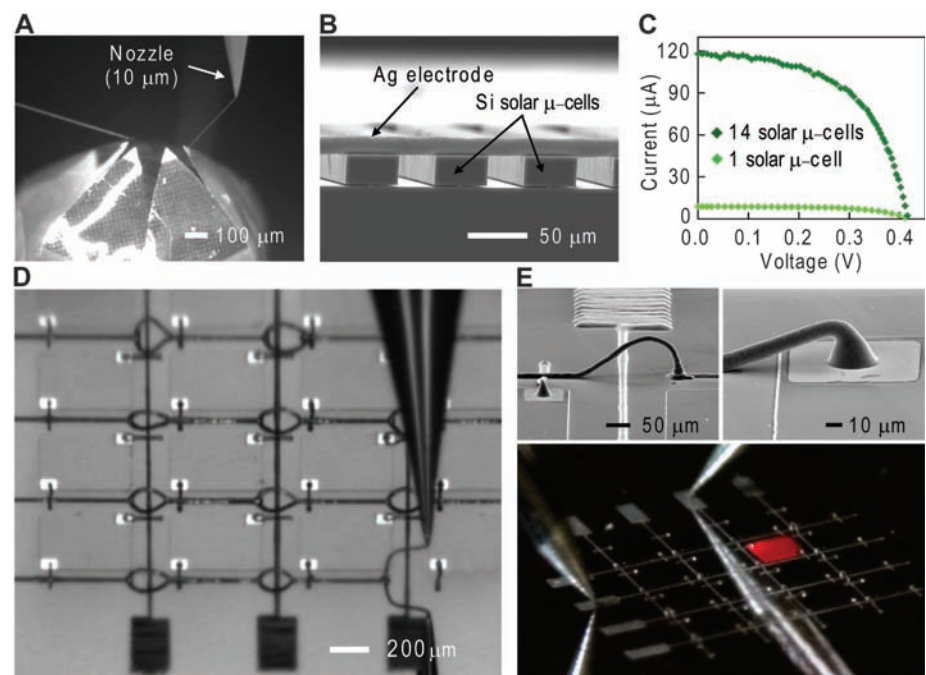


**Fig. 4.** (A) Optical image obtained during wire bonding onto a thin (2- $\mu\text{m}$ ) silicon spherical shell using a 10- $\mu\text{m}$  nozzle. (B) Optical image of a spanning silver microelectrode printed onto an unplanarized, silicon solar microcell array. (C) Current ( $I$ )–voltage ( $V$ ) response of an individual silicon solar microcell and a 14-microcell array connected by silver microelectrodes. (D) Optical image acquired during patterning of silver interconnects on a gallium arsenide–based, 4-by-4 LED chip array. (E) A silver interconnect arch printed over an electrode junction (top left) and on a gold contact pad (80 by 80  $\mu\text{m}$ ) (top right) and an optical image of light emission from a single LED pixel in the  $y = 2$ ,  $x = 3$  position within the array under an applied voltage (bottom).

the silver nanoparticle concentration, size, and distribution, we have produced inks with high solids loading ( $\geq 70$  wt %) that are ideally suited for direct-write assembly. We have shown that self-supporting microelectrodes in either planar or 3D forms of arbitrary complexity can be patterned on a wide variety of substrates. Using this technique, we have further demonstrated the feasibility of wire bonding to fragile devices and patterning complex interconnects for solar cell and LED arrays.

#### References and Notes

- D. B. Chrisey, *Science* **289**, 879 (2000).
- H. Sirringhaus *et al.*, *Science* **290**, 2123 (2000).
- S. R. Forrest, *Nature* **428**, 911 (2004).
- Y. Sun, J. A. Rogers, *Adv. Mater.* **19**, 1897 (2007).
- E. Menard *et al.*, *Chem. Rev.* **107**, 1117 (2007).
- M. C. LeMieux *et al.*, *Science* **321**, 101 (2008).
- Q. Cao *et al.*, *Nature* **454**, 495 (2008).
- J. Yoon *et al.*, *Nat. Mater.* **7**, 907 (2008).
- J. A. Rogers *et al.*, *Proc. Natl. Acad. Sci. U.S.A.* **98**, 4835 (2001).
- V. Subramanian *et al.*, *Proc. IEEE* **93**, 1330 (2005).
- R. A. Potyrailo, W. G. Morris, *Anal. Chem.* **79**, 45 (2007).
- M. Hosokawa, K. Nogi, M. Naito, T. Yokoyama, *Nanoparticle Technology Handbook* (Elsevier, Oxford, ed. 1, 2007).
- T. H. J. van Osch, J. Perelaer, A. W. M. de Laat, U. S. Schubert, *Adv. Mater.* **20**, 343 (2008).
- J. E. Smay, J. Cesarano III, J. A. Lewis, *Langmuir* **18**, 5429 (2002).
- Q. Li, J. A. Lewis, *Adv. Mater.* **15**, 1639 (2003).
- Y. Sun, Y. Xia, *Science* **298**, 2176 (2002).
- B. Wiley, Y. Sun, Y. Xia, *Acc. Chem. Res.* **40**, 1067 (2007).
- M. Yamamoto, Y. Kashiwagi, M. Nakamoto, *Langmuir* **22**, 8581 (2006).
- A. Pyatenko, M. Yamaguchi, M. Suzuki, *J. Phys. Chem. C* **111**, 7910 (2007).
- B.-H. Ryu *et al.*, *Colloids Surf. A Physicochem. Eng. Asp.* **270–271**, 345 (2005).
- Materials and methods are available as supporting material on Science Online.
- M. Dobbelin *et al.*, *Chem. Mater.* **19**, 2147 (2007).
- J. Ouyang *et al.*, *Polymer* **45**, 8443 (2004).
- T. Li, Z. Huang, Z. Suo, S. P. Lacour, S. Wagner, *Appl. Phys. Lett.* **85**, 3435 (2004).
- D.-Y. Khang, H. Jiang, Y. Huang, J. A. Rogers, *Science* **311**, 208 (2006); published online 14 December 2005 (10.1126/science.1121401).
- G. G. Harman, *Wire Bonding in Microelectronics: Process, Reliability, and Yield* (McGraw-Hill Professional, New York, 1997).
- J.-H. Ahn *et al.*, *Science* **314**, 1754 (2006).
- S. Ashley, *Sci. Am.* **299**, 32 (2008).
- This material is based on work supported by the U.S. Department of Energy, Materials Sciences and Engineering Division under award no. DEFG-02-07ER46471, through the Frederick Seitz Materials Research Laboratory (FSMRL) at the University of Illinois. The authors gratefully acknowledge use of the FSMRL Central Facilities, including Center for Microanalysis of Materials. B.Y.A. thanks the Korean Research Foundation for the postdoctoral fellowship. We also thank C. Hansen, M. Xu, R. Shepherd, J. Bukowski, J. Carroll III, and J. Yoshikawa for useful discussions. J.A.L., B.Y.A., and E.B.D. submitted a U.S. patent application on this work entitled "Metal Nanoparticle Inks" on 3 October 2008.

#### Supporting Online Material

www.sciencemag.org/cgi/content/full/1168375/DC1  
Materials and Methods

Figs. S1 to S9

References

11 November 2008; accepted 27 January 2009

Published online 12 February 2009;

10.1126/science.1168375

Include this information when citing this paper.

# A Meta-Selective Copper-Catalyzed C–H Bond Arylation

Robert J. Phipps and Matthew J. Gaunt\*

For over a century, chemical transformations of benzene derivatives have been guided by the high selectivity for electrophilic attack at the ortho/para positions in electron-rich substrates and at the meta position in electron-deficient molecules. We have developed a copper-catalyzed arylation reaction that, in contrast, selectively substitutes phenyl electrophiles at the aromatic carbon–hydrogen sites meta to an amido substituent. This previously elusive class of transformation is applicable to a broad range of aromatic compounds.

Aromatic organic compounds are ubiquitous in modern society as medicines and functionalized materials (1). These molecules comprise cyclic aryl cores with an often complex array of substituents on the ring carbons, which in many cases are most straightforwardly appended by electrophilic substitution (2). Ever since the pioneering work of Friedel and Crafts (3), it has been widely established that electron-donating substituents direct incoming electrophiles to the ortho and para positions, whereas electron-withdrawing groups steer to the meta position (Fig. 1A). This fundamental reactivity pattern facilitates a predictable outcome in simple cases; however, a common problem encountered in synthesis is how to access the isomer that is not anticipated by these rules. Solutions to this problem often require numerous functional group additions or manipulations in order to tailor the directing electronic properties of the precursor to furnish the desired product.

Furthermore, in complex systems, where there may be more than one electronic or sterically active substituent, the competition between these directing groups may lead to mixtures of products. Although there have been some reports that indirectly address these problems (4–7), circumventing the inherent ortho/para-selectivity of electron-rich aromatic systems to generate the meta product remains a largely elusive and unmet goal for chemical synthesis.

A central theme of our research has been the development of methods to obviate reliance on complex functional group manipulations through direct metal-catalyzed C–H bond transformations (8, 9). A key aspect of this goal is the ability to control the site selectivity of these transformations under mild conditions; a challenge that is further complicated by the ubiquitous nature of the C–H bond in organic molecules (10–15). The three mechanisms that usually rationalize the majority of selective metal-catalyzed C–H bond activation methods involve electrophilic aromatic substitution with electron-rich,  $\pi$ -nucleophilic arenes (16), concerted metalation-deprotonation with simple and electron-deficient benzenes (17–19), and directed cyclometalation (20–26). These mecha-

nistic pathways most commonly form the ortho-substitution product, and as a result there is a paucity of methods for metal-catalyzed C–H bond activation at the meta position of a substituted benzene ring (27, 28).

Here we describe the development of a reactivity concept for a metal-catalyzed aromatic C–H bond functionalization strategy that selectively generates the elusive meta isomer. The outcome is not predicted by the conventional rules associated with electronic factors, directing groups, or steric effects, and provides direct access to the meta isomer on highly versatile electron-rich aromatic structures. The process is simple, proceeds under mild conditions, uses inexpensive copper catalysts, and forms valuable products that would be difficult to synthesize by other methods (Fig. 1B). Furthermore, the reactivity and selectivity of this process should be compatible with other arene and C–H bond transformations and will streamline synthetic strategy for the assembly of medicines, natural products, and industrially relevant aromatic molecules.

We previously identified a copper catalysis system, based on electrophilic metalation, that enables site-selective C–H bond arylation on the indole skeleton (Fig. 2A) (10). We speculated that a Cu(I) catalyst is oxidized to a Cu(III)-aryl intermediate (29), a highly electrophilic  $d^8$ -configured metal species, that undergoes Friedel-Crafts-type metalation and arylation at the C3 position of the indole (Fig. 2B). We see C3 arylation when using our copper catalyst, whereas an almost identical process using Pd(II)-salts delivers the C2 isomer (30). Although the origin of this dichotomy remains unclear, it led us to speculate that use of our copper catalyst might enable us to reverse the established selectivity of other electrophilic Pd(II)-catalyzed transformations. For example, many Pd(II)-catalyzed reactions are ortho-selective and have been routinely developed by virtue of the coordinat-

Department of Chemistry, University of Cambridge, Lensfield Road, Cambridge CB2 1EW, UK.

\*To whom correspondence should be addressed. E-mail: mjj32@cam.ac.uk



[www.sciencemag.org/cgi/content/full/1168375/DC1](http://www.sciencemag.org/cgi/content/full/1168375/DC1)

Supporting Online Material for  
**Omnidirectional Printing of Flexible, Stretchable, and Spanning Silver  
Microelectrodes**

Bok Y. Ahn, Eric B. Duoss, Michael J. Motala, Xiaoying Guo, Sang-Il Park, Yujie Xiong, Jongseung Yoon, Ralph G. Nuzzo, John A. Rogers, Jennifer A. Lewis\*

\*To whom correspondence should be addressed. E-mail: [jalewis@illinois.edu](mailto:jalewis@illinois.edu)

Published 12 February 2009 on *Science Express*  
DOI: 10.1126/science.1168375

**This PDF file includes:**

Materials and Methods  
Figs. S1 to S9  
References

# Omnidirectional Printing of Flexible, Stretchable, and Spanning Silver Microelectrodes

Bok Y. Ahn,<sup>1,2</sup> Eric B. Duoss,<sup>1,2</sup> Michael J. Motala,<sup>1,3</sup> Xiaoying Guo,<sup>1,2</sup> Sang-Il Park,<sup>1,2</sup> Yujie Xiong,<sup>1,2</sup> Jongseung Yoon,<sup>1,2</sup> Ralph G. Nuzzo,<sup>1,3</sup> John A. Rogers,<sup>1,3</sup> and Jennifer A. Lewis<sup>1,2\*</sup>

<sup>1</sup>Frederick Seitz Materials Research Laboratory, University of Illinois at Urbana-Champaign, Urbana, Illinois 61801, USA

<sup>2</sup>Department of Materials Science and Engineering, University of Illinois at Urbana-Champaign, Urbana, Illinois 61801, USA

<sup>3</sup>Department of Chemistry, University of Illinois at Urbana-Champaign, Urbana, Illinois 61801, USA

## MATERIALS AND METHODS

### Silver Nanoparticle Inks

Silver nanoparticle inks are prepared by first dissolving 2 g poly(acrylic acid) (PAA) solution (50 wt% polymer in water, molecular weight = 5,000 g/mol), 1 g PAA (25 wt% polymer in water, molecular weight = 50,000 g/mol), and 40 g diethanolamine (DEA) in 50 ml of H<sub>2</sub>O, while stirring for 2 h in a water bath at room temperature (Fig. S1-A). The solution pH is 9.5 (Fig. S1-B). A silver nitrate solution (20 g AgNO<sub>3</sub> in 20 ml H<sub>2</sub>O) is then added to this solution, while vigorously stirring, to yield weight ratios of DEA/Ag and PAA/Ag of 3.15 and 0.089, respectively. The resulting reddish-yellow solution (Fig. S1-C) is then gently stirred for 24 h at room temperature. The solution exhibits a gradual color change from reddish-yellow to dark black, which coincides with the formation of silver nanoparticles that are ~ 5 nm in diameter, as determined by transmission electron microscopy (JOEL 2010Lab6 TEM, JEOL Ltd.). The silver nanoparticles are ripened by sonicating the solution in a heated water bath at 60°C for 2 h (Fig. S1-D). After this step,

the mean particle size is  $\sim 20 \pm 5$  nm with a size distribution between 5 – 50 nm. The resulting silver nanoparticles are concentrated by titrating 240 ml ethanol at  $10 \text{ ml min}^{-1}$ . Because ethanol is a poor solvent for the PAA-coated silver nanoparticles, rapid coagulation ensues. After decanting the supernatant, the coagulated ink is centrifuged at 9,000 rpm for 20 min to remove excess solvent and recover the precipitate (Fig. S1-E). The process yields a highly concentrated silver nanoparticle ink with a solids loading of  $\sim 81$  wt%. The resultant ink is then homogenized by adding  $\sim 10$  wt% of a humectant solution (30 wt% ethylene glycol/70 wt% water) followed by deairing for  $\sim 30$  min under a light vacuum (ca. 25 mbar) until bubble formation ceases. After homogenization, the ink changes from a bluish to a magenta color (Fig. S1-F). Note, the homogenized ink readily flows through fine deposition nozzles (1 – 30  $\mu\text{m}$  in diameter), is stable under ambient conditions for weeks, and can be easily redispersed in water or ethylene glycol to form a low viscosity solution.

The ink rheology is measured in both shear viscometry and oscillatory mode using a controlled-stress rheometer (C-VOR, Malvern Instruments, Malvern, UK) equipped with either a cup and bob (C8, 8 mm bob diameter and 0.4 mm gap width) or cone and plate geometry (CP4/40, 40 mm cone diameter with a  $4^\circ$  angle and 0.15 mm gap width) at  $25^\circ\text{C}$  in the presence of solvent trap to prevent evaporation. The apparent viscosity ( $\eta$ ) is acquired as a function of shear rate ( $0.01 - 30 \text{ s}^{-1}$ ) in a logarithmically ascending series. The elastic shear ( $G'$ ) and viscous loss ( $G''$ ) moduli are measured in oscillatory mode as a function of controlled shear stress (0.8 - 2,000 Pa) at a frequency of 1 Hz with increasing amplitude sweep.

The ink solids loading, defined by the silver nanoparticle concentration in wt%, is determined using thermogravimetric analysis (Mettler Toledo TGA/SDTA851, Columbus, OH), in which the sample is heated at  $10^{\circ}\text{C min}^{-1}$  to  $800^{\circ}\text{C}$  in air (Fig. S1-I).

### **Omnidirectional Printing**

Omnidirectional printing is carried out using a 3-axis micropositioning stage (ABL 900010, Aerotech Inc., Pittsburgh, PA), whose motion is controlled by computer-aided design software (RoboCAD, 3D Inks, Stillwater, OK) (*SI*). The silver ink is housed in a syringe (3 mL barrel, EFD Inc., East Providence, RI) attached by luer-lok to a borosilicate micronozzle (diameter = 1 – 30  $\mu\text{m}$  produced using a P-2000 micropipette puller, Sutter Instrument Co., Novato, CA). An air-powered fluid dispenser (800 ultra dispensing system, EFD Inc.) is used to pressurize the barrel and control the ink flow rate. The required pressure depends upon ink rheology, nozzle diameter, and printing speed, but typical values range from 10 – 100 psi at 20 – 500  $\mu\text{m s}^{-1}$ . Omnidirectional printing is performed in air under ambient conditions at a relative humidity of  $\sim 20 - 30\%$  and temperature of 23 – 26 $^{\circ}\text{C}$ .

### **Planar Silver Microelectrodes**

Both planar and multilayer silver microelectrodes are patterned in a layerwise build sequence, in which the nozzle height is raised a distance ( $z$ ) that is proportional to the nozzle diameter ( $d$ ). Typically,  $z \sim 0.8d$  ensures good adhesion between the printed layers. The printed silver microelectrodes are heated in air at  $10^{\circ}\text{C min}^{-1}$  to the desired annealing temperature of 150 – 550 $^{\circ}\text{C}$  for varying times. Their electrical resistivity is measured using micropositioners (Signatone) with tungsten tips (SE-T, Signatone) attached to a source meter (Keithley 2400). Silver microelectrode morphology is observed using a

scanning electron microscope (SEM, JOEL 6060LV, JEOL Ltd.) after sputtering with Au/Pd for 30 s (Emitech K575 Sputter Coater). The aspect ratio (height/width,  $h/w$ ) of the silver microelectrodes is determined by surface profilometry (Veeco Instrument, Dektak 3030) or SEM microscopy.

### **Flexible and Stretchable Silver Microelectrodes**

An array of ten silver microelectrodes ( $w = 21 \mu\text{m}$ ,  $h = 12 \mu\text{m}$ , and length,  $l = 1 \text{ cm}$ ) spaced 0.5 mm apart are printed using a  $20 \mu\text{m}$  nozzle onto a  $25 \mu\text{m}$  thick polyimide substrate (Kapton, CS Hyde Co.) with contact pads ( $0.3 \text{ mm} \times 0.3 \text{ mm}$ ) deposited at each end for electrical characterization. The contact pads are created by translating the nozzle in the  $x$ - $y$  plane, such that the center-to-center distance between adjacent deposited features is less than the nozzle diameter, to produce continuous (solid) features. The printed features are then annealed at  $200^\circ\text{C}$  for 3 h in air. To evaluate the effects of mechanical bending on their electrical performance, we carried out bend tests using a custom-built mechanical stage coupled to a micropositioner (Fig. S3-A). The electrical resistivity ( $\rho$ ) of these microelectrodes is measured as a function of bending radius for tensile (convex), unstrained (flat), and compressive (concave) states. The average values of the electrical resistivity are reported as a function of bending radius ( $\pm 11 \text{ mm}$  to  $\pm 5 \text{ mm}$ ) for the initial testing cycle, and as a function of bending cycle (up to 1,000 cycles) for the unstrained, maximum tensile and compressive states ( $\pm 5 \text{ mm}$ ). For the microelectrodes tested, all 10 survived 500 bending cycles, 9 survived 750 bending cycles, and 5 survived 1,000 bending cycles.

Stretchable microwires are produced by printing a linear silver microelectrode onto a pre-strained spring, with gaps between spring elements of  $L_{print}$ . After releasing the

strain, microwire arches form spontaneously. The resultant arches are heated in air at  $10^{\circ}\text{C min}^{-1}$  to the desired annealing temperature of  $200 - 550^{\circ}\text{C}$ , held for 3 h, and then furnace cooled. To ensure accurate resistivity measurements, approximately 500 pL of a thermally curable silicone (Silicon Solutions, SS-4061,  $\eta = 0.9 \text{ Pa}\cdot\text{s}$ ) is subsequently deposited through a  $100 \mu\text{m}$  nozzle onto the spring at each microelectrode contact joint. The coating, which serves as both an insulation and adhesion layer, is cured by heating the patterned samples in air at  $150^{\circ}\text{C}$  for 30 min. The resistivity of the microwire arches as function of strain,  $[(L-L_0)/L_0 \times 100\%]$ , where  $L < L_{print}$ , is measured using the custom-designed strain stage coupled to a micropositioner, as shown in Fig. S3-B (S2).

### **Spanning Silver Interconnects to Thin Silicon Spherical Shells**

Thin silicon spherical shells are fabricated from a silicon-on-insulator (SOI) wafer (Ultrasil Corp.) through a combination of photolithography, etching, and folding techniques. Details of 3D folding procedure for silicon or metal-polymer thin film structures are published elsewhere (S3,4). The fabrication process for these objects consists of three steps. First, a 6-point star-shaped 2D silicon pattern ( $2 \mu\text{m}$  thick, 8 mm end-to-end length) is photolithographically defined on the wafer and the remaining silicon is etched away by  $\text{SF}_6$  plasma (Plasma Therm) (Fig. S5-A). This 2D pattern is then released by etching with concentrated hydrofluoric acid (49% HF). To facilitate the etching process, the silicon is lithographically patterned with  $4 \mu\text{m}$  diameter holes that are spaced  $40 \mu\text{m}$  apart with respect to their center-to-center separation distance. After rinsing in acetone, the 2D structure is transferred on a Teflon substrate and a PVA-coated glass ball (2.38 mm diameter) is placed in the center of the structure. Finally, the

structure is folded to the desired 3D spherical shell by depositing a water droplet on the structure and allowing it to dry at room temperature for 2 h (Fig. S5-B).

Silver interconnects are wire-bonded to these 3D spherical shells by omnidirectional printing using a 10  $\mu\text{m}$  nozzle (Fig. S5-C). First, a silver electrode and pad (1 mm  $\times$  1 mm) are printed on a glass substrate and the 3D spherical shell is placed on the pad. The printed pad serves as both the electrode and adhesive. Next, a spanning silver electrode is printed as a top electrode by omnidirectional printing, followed by annealing at 200°C for 3 h. Due to their delicate nature, careful handling of the 3D object is required to avoid fracture upon physical contact with the nozzle. Note, no cracks or deformation occurred during the wire-bonding process (Fig. S5-D).

### **Spanning Silver Interconnects to Silicon Solar Microcells**

Silicon solar microcells (Fig. S6-A) are fabricated from *n*-type (phosphorous), single-crystalline silicon wafer (Virginia Semiconductor, Inc., Si  $\langle 111 \rangle \pm 0.1$ ,  $\rho = 0.1 - 1 \Omega\cdot\text{cm}$ ). Details of the fabrication process have been described previously (S5,6). In brief, the top surface of the wafer is doped with phosphorous using a spin-on-dopant (SOD) source (P8454 SF2.7, Filmtronics Inc.). After doping, the residual SOD and undesirable phosphosilicate glass (PSG) is etched. An oxide layer ( $\sim 300$  nm) is then grown by PECVD (Plasma Therm, Unaxis SLR730), followed by spin-coating with photoresist (AZ 5214, Clariant). The silicon ribbon pattern is aligned lengthwise perpendicular to the Si  $\langle 110 \rangle$  direction for the photolithographic and etching process. The photoresist is developed, oxide windows opened, and the silicon vertically etched by ICP RIE (STS Mesc Multiplex, Advanced Si Etcher), resulting in the silicon microribbons. The top and sides of the silicon microribbons are first protected and then under-cut by anisotropic

etching of the <110> plane with tetramethylammonium hydroxide (TMAH, Aldrich). A boron emitter is then formed on the underside of the ribbons by spinning several layers of a polyboron SOD (PBF6M-25, Filmtronics Inc.). After doping and cleaning, the desired silicon solar microcell arrays are obtained.

The silicon solar microcell array is interconnected in parallel (Fig. S6-B,C). This is achieved by first electron-beam (e-beam) deposition (Temescal, FC 1800) of a thin Ti/Au (10 Å/50 Å) contact (75 µm wide) through a shadow mask across a cell row. The thin metal layer is used to ensure ohmic contact with the underlying silicon solar microcell surfaces. The top electrode is formed by printing the silver ink onto the titanium (Ti)/(Au) contacts. This electrode is then heated in air at 10°C min<sup>-1</sup>, and annealed at 250°C for 3 h to produce an ohmic contact. To form the bottom electrodes, the cells are transfer-printed (S7) onto a patterned gold grid (4 µm wide, 100 nm thick, 40 µm center-to-center spacing) supported on a PDMS-coated glass substrate. The device is characterized by measuring its current (*I*)-voltage (*V*) response under Air Mass 1.5 (AM 1.5) illumination at 1000 W m<sup>-1</sup> using a Keithley 2400 source meter.

### **Spanning Silver Interconnects to Light Emitting Diodes**

Silver interconnects are wire-bonded to a commercial gallium nitride (GaN), light emitting diode (LED) (Three Five Compounds Inc., 1 mm × 1mm × 200 µm) by omnidirectional printing. First, a planar silver electrode with a pad (500 µm × 500 µm) is printed on a glass substrate, followed by placing the LED chip (with a gold contact on the back) on the pad. The printed pad serves as both the electrode and adhesive. Next, a silver arch is printed as a top electrode by omnidirectional printing (Fig. S8-A). The patterned device is then annealed at 200°C for 3 h in air. The device is characterized by

measuring its current ( $I$ )-voltage ( $V$ ) response using a semiconductor parameter analyzer (Keithley 2400). Light emission images (Fig. S8-B) are taken with digital still camera (Canon EOS-1Ds Mark III).

As a final example, silver interconnects are patterned by omnidirectional printing on a  $4 \times 4$  LED array, whose fabrication begins with a GaAs wafer (Epiworks, Inc.) composed of a 500 nm thick bottom Si-doped GaAs  $n$ -contact layer, a 800 nm thick Si-doped  $n$ -Al<sub>0.45</sub>Ga<sub>0.55</sub>As current-spreading layer, an 18 nm InGaP-based active region, a 800 nm thick C-doped  $p$ -Al<sub>0.45</sub>Ga<sub>0.55</sub>As current-spreading layer, and a 5 nm thick top C-doped  $p$ -contact layer (Fig. S9-A) (S8). An array of LED cells ( $500 \mu\text{m} \times 500 \mu\text{m}$ ) are defined by spin coating, exposing (Karl Suss MJB mask aligner, i-line), and developing (AZ327MIF, Clariant) photoresist (AZ5214, Clariant). The LED cells are isolated by a 3-step wet etching process ( $p$ -GaAs: H<sub>3</sub>PO<sub>4</sub>/H<sub>2</sub>O<sub>2</sub>/H<sub>2</sub>O, InGaP-based active region: HCl/H<sub>2</sub>O,  $n$ -GaAs: H<sub>3</sub>PO<sub>4</sub>/H<sub>2</sub>O<sub>2</sub>/H<sub>2</sub>O). The bottom GaAs  $n$ -contact layers in the corner of the LED cells are exposed to form a contact pad using photolithography and wet etching, akin to the above process except that the  $n$ -contact layers are not etched. The  $p$ - and  $n$ -contact pads ( $80 \mu\text{m} \times 80 \mu\text{m}$ ) on the LED cells are formed by depositing Ti (7 nm) and Au (100 nm) in an e-beam evaporator (Temescal, FC 1800) and followed by photoresist lift-off processing (Fig. S9-B). A complex pattern of silver interconnects is then produced by omnidirectional printing using a  $10 \mu\text{m}$  nozzle, as shown in Fig. S9-C. First, the silver arches are patterned for both  $n$ - and  $p$ -contact pads. Next, the printed silver arches in the  $n$ -sides are connected by printing planar electrodes. Finally, the printed arches in the  $p$ -area are connected. No insulation layers are required, because this novel arch layout avoids undesired contacts between patterned microelectrodes. Silver contact pads (200

$\mu\text{m} \times 900 \mu\text{m}$ ) are printed for electrical measurements and to individually address each LED pixel within the  $4 \times 4$  array. The patterned device is then annealed at  $200^\circ\text{C}$  for 3 h in air.

## SUPPORTING FIGURES

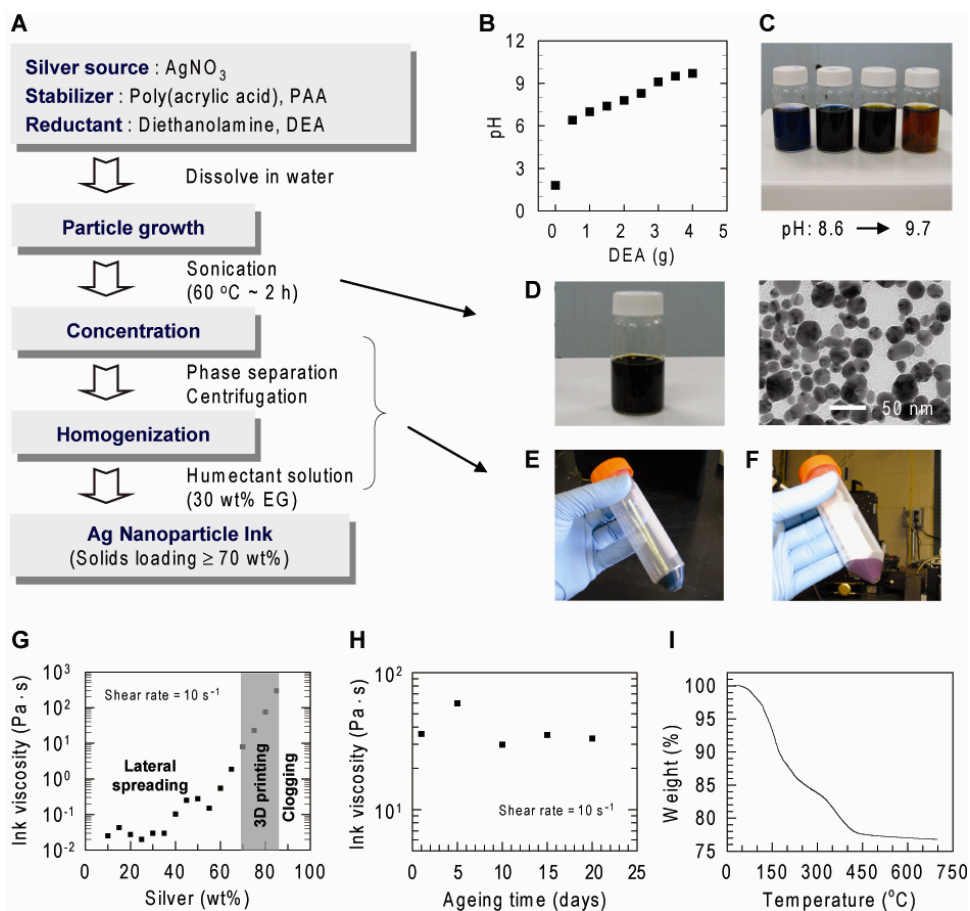


**Fig. S1.** (A) A flow diagram of the ink preparation procedure using an aqueous  $\text{AgNO}_3$ /PAA/DEA system. (B) Solution pH as a function of DEA in solution (10g  $\text{H}_2\text{O}$ , 2g  $\text{AgNO}_3$ , and 0.14g PAA). (C) Optical images of solutions at different pH. (D) Optical image (left) of the solution after sonication at 60°C for 2 h and TEM micrograph (right) of the ripened silver nanoparticles harvested from solution. (E) Silver nanoparticle ink obtained by centrifugation at 9,000 rpm for 20 min. (F) Silver nanoparticle ink after homogenization by adding a 5 wt% humectant solution composed of 30 wt% ethylene glycol in water. (G) Ink viscosity as a function of silver nanoparticle concentration. (H) Ink viscosity as a function of ageing time. (I) Thermogravimetric analysis of a silver nanoparticle ink (77 wt% solids) prepared by this procedure.

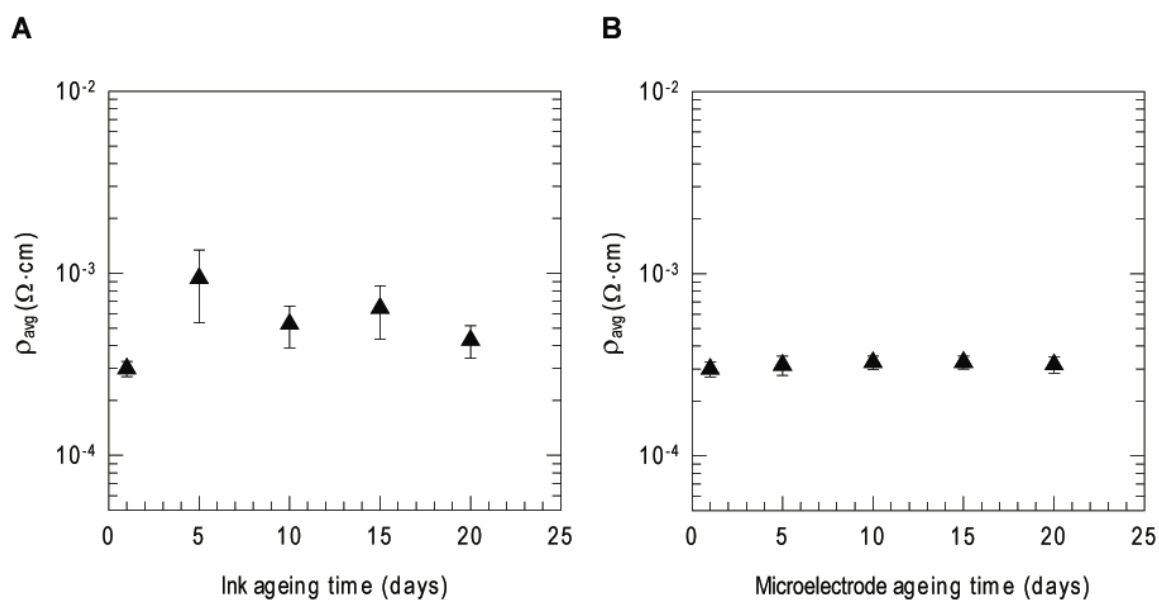


**Fig. S2.** (A) Electrical resistivity of the printed silver microelectrodes as a function of ink ageing time at room temperature. (B) Electrical resistivity of the silver microelectrodes as a function of microelectrode ageing time at room temperature in air.

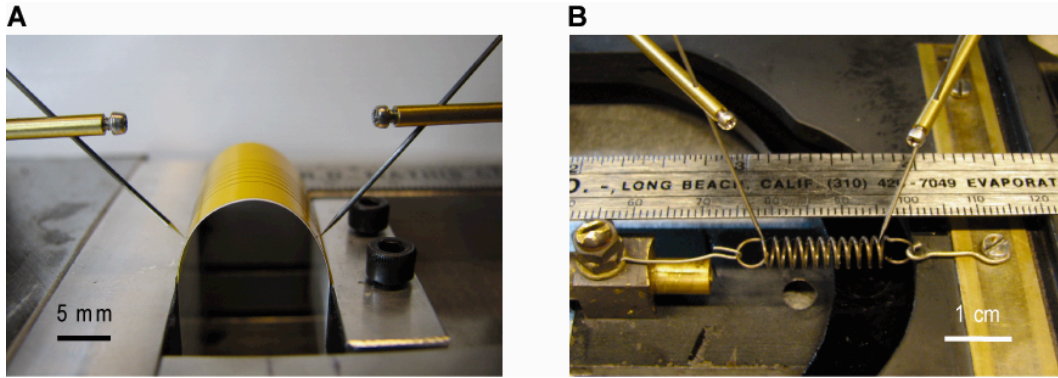


**Fig. S3.** (A) Optical image of the bend test apparatus for measuring the electrical resistivity of silver microelectrodes. (B) Optical image of the strain test apparatus for measuring the electrical resistivity of spanning silver arches.

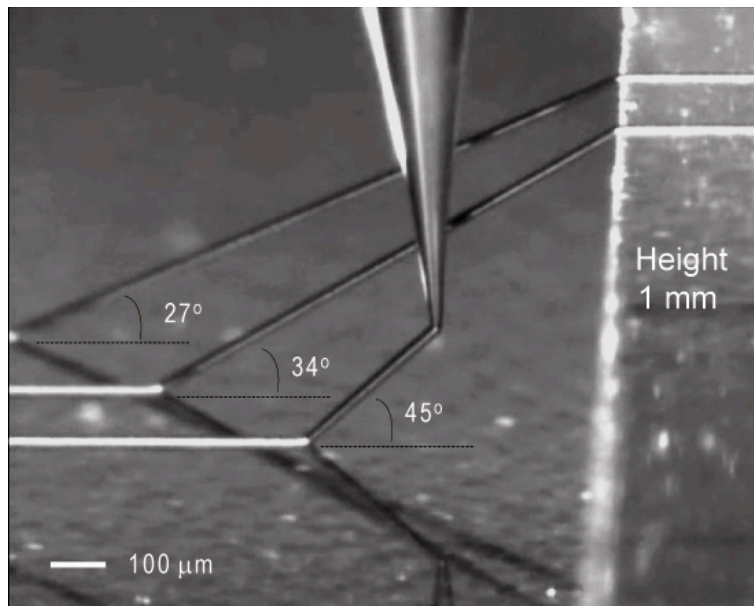


**Fig. S4.** Optical image acquired during omnidirectional printing of silver microelectrodes between two glass substrates offset by a 1 mm height difference.

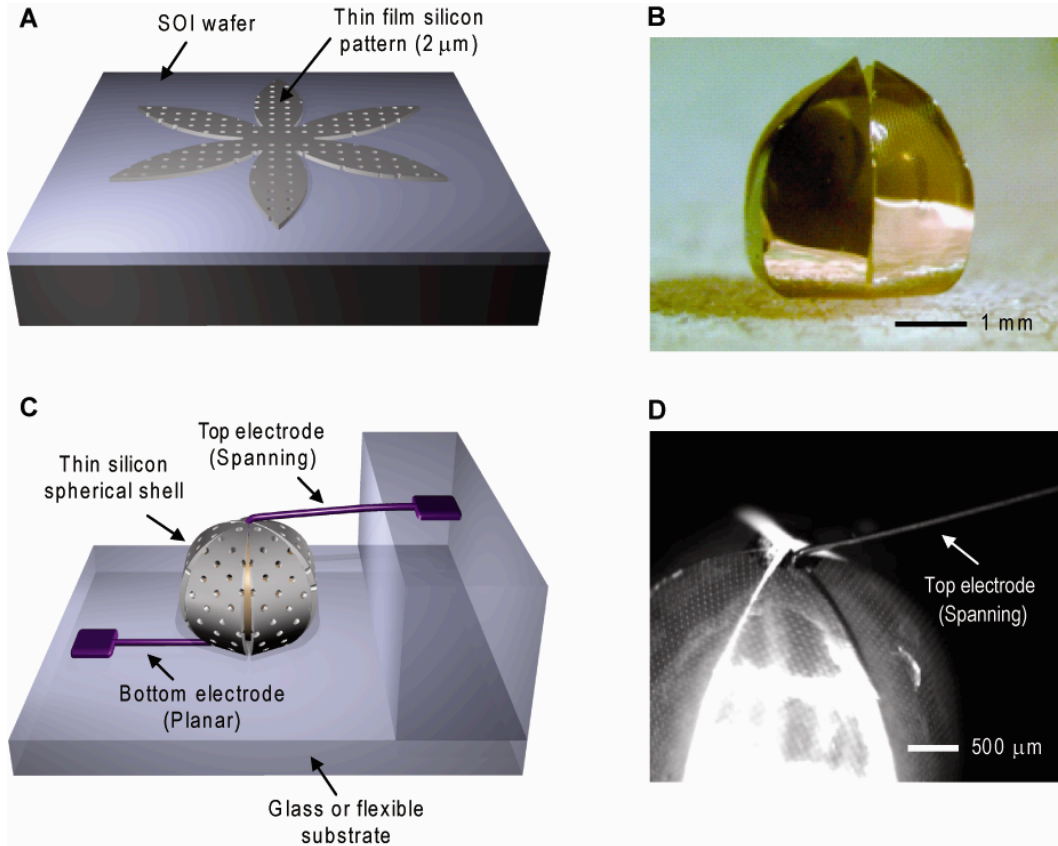


**Fig. S5.** (A) Schematic diagram of thin film silicon photolithographically patterned on a SOI wafer. (B) Optical image of 3D silicon spherical shell folded from the thin film silicon pattern after etching and release. (C) Schematic diagram illustrating the wire-bonding of silver microelectrodes onto a thin silicon spherical shell by omnidirectional printing. (D) SEM image of a spanning silver microelectrode wire-bonded onto this 3D object.

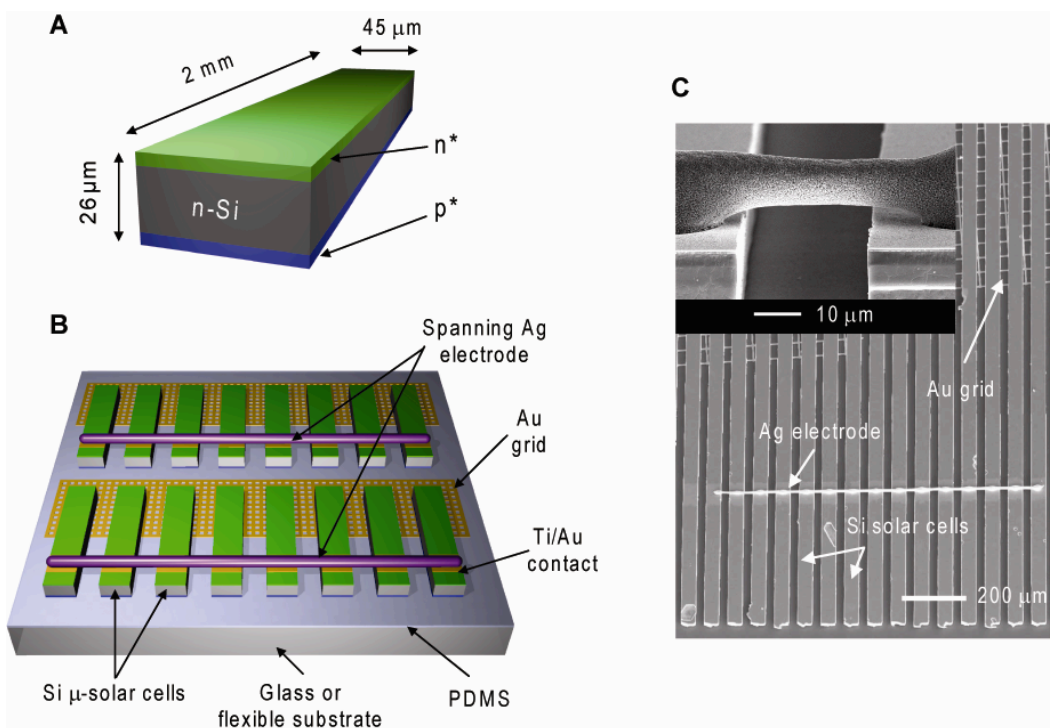


**Fig. S6.** (A) Schematic diagram of an individual silicon microcell composed of a  $p$ - $n$  junction. (B) Schematic diagram of an interconnected, silicon solar microcell array. (C) SEM image of this solar microcell array, in which a high magnification image of the spanning silver microelectrode is provided as an inset.

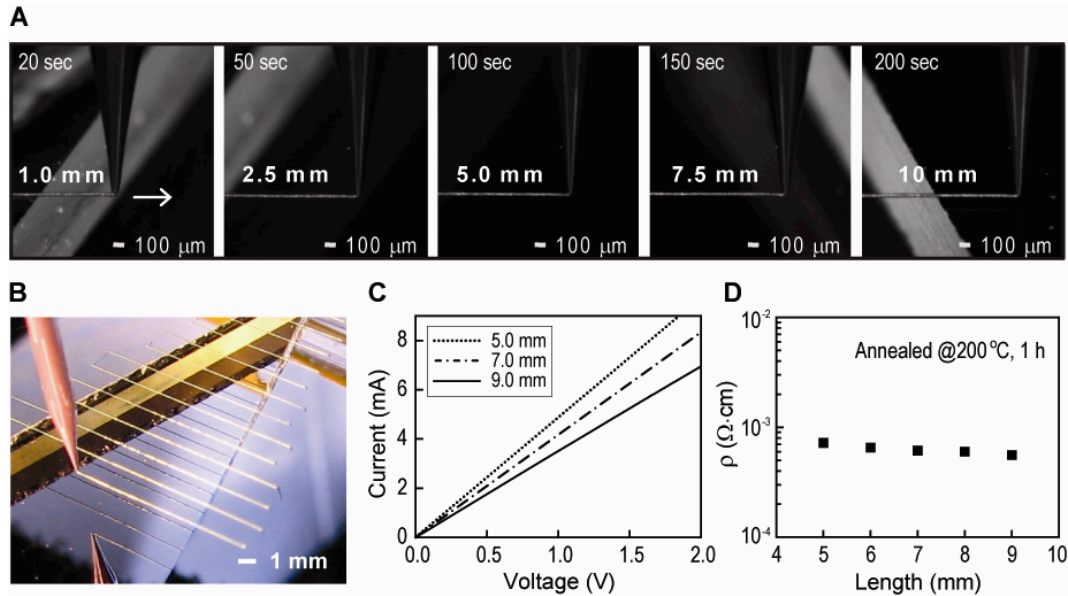


**Fig. S7.** (A) Optical images acquired during direct writing of silver microelectrodes using a 10  $\mu$ m nozzle, which span long distances ( $\geq 1.0$  cm). (B) Optical image of spanning silver microelectrodes printed over a wedge-shaped gap with 1 mm height difference between top and bottom surfaces. (C) Current ( $I$ )-voltage ( $V$ ) characteristics of the spanning silver microelectrodes as a function of length. (D) Electrical resistivity ( $\rho$ ) of the silver microelectrodes as a function of their length.

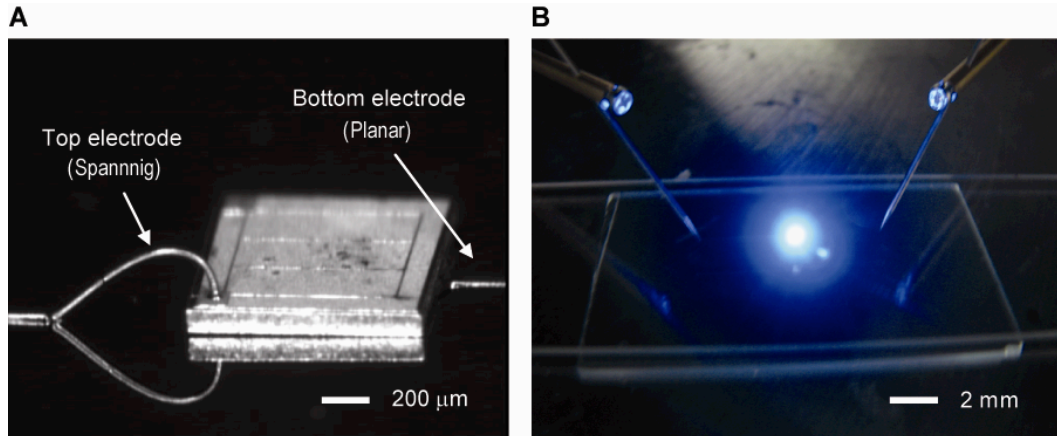


**Fig. S8.** (A) Optical image of a gallium nitride (GaN) LED chip ( $1\text{ mm} \times 1\text{ mm} \times 200\text{ }\mu\text{m}$ ) connected by a bottom electrode composed of a silver pad with planar line and a top electrode composed of a spanning silver microelectrode, both of which are patterned by omnidirectional printing. (B) Optical image of the LED chip emitting blue light (469 nm) under an applied bias of  $2\text{ V}$ , after annealing at  $200^\circ\text{C}$  for 3 h.

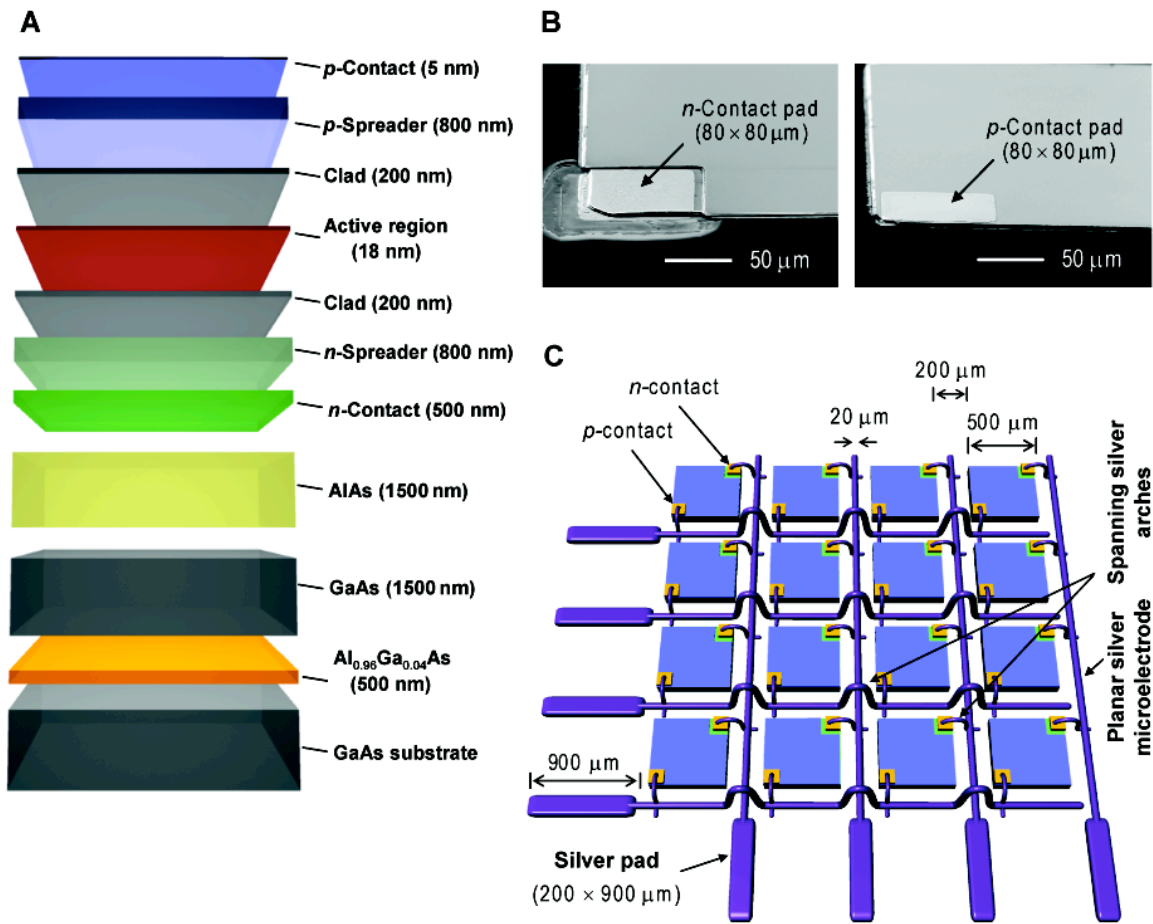


**Fig. S9.** (A) Multilayer composition of the GaAs wafer used for fabricating individual LED cells within the  $4 \times 4$  array. (B) SEM images of  $n$ - and  $p$ -contact pads in an LED cell. (C) A schematic diagram of the  $4 \times 4$  LED array interconnected by silver microelectrodes patterned by omnidirectional printing.

## REFERENCES

- S1. R. B. Rao, K. L. Krafcik, A. M. Morales, J. A. Lewis, *Adv. Mater.* **17**, 289 (2005).
- S2. Y. Sun, W. M. Choi, H. Jiang, Y. Y. Huang, J. A. Rogers, *Nature Nanotech.* **1**, 201 (2006).
- S3. D. H. Gracias, V. Kavthekar, J. C. Love, K. E. Paul, G. M Whitesides, *Adv. Mater.* **14**, 235 (2002).
- S4. D. H. Gracias, J. Tien, T. L. Breen, C. Hsu, G. M. Whitesides, *Science* **289**, 1170 (2002)
- S5. J. Yoon et al., *Nature Mater.* **17**, 907 (2008).
- S6. A. J. Baca et al., *Adv. Funct. Mater.* **17**, 3051 (2007).
- S7. X. Feng et al., *Langmuir* **23**, 12555 (2007).
- S8. T. Kim et al., *IEEE Photon. Technol. Lett.* **18**, 1876 (2006).